PHILOSOPHICAL TRANSACTIONS OF THE ROYAL SOCIETY A

rsta.royalsocietypublishing.org

Research

Cite this article: Jiao F, Di C-a, Sun Y, Sheng P, Xu W, Zhu D. 2014 Inkjet-printed flexible organic thin-film thermoelectric devices based on p- and n-type poly(metal 1,1,2,2-ethenetetrathiolate)s/polymer composites through ball-milling. *Phil. Trans. R. Soc. A* **372**: 20130008.
http://dx.doi.org/10.1098/rsta.2013.0008

One contribution of 8 to a Theo Murphy Meeting Issue 'Theo Murphy International Scientific Meeting between the UK and China on the chemistry and physics of functional materials'.

Subject Areas:
materials science, power and energy systems

Keywords:
thermoelectric, film, metal coordination polymers, composite, ball-milling, inkjet printing

Authors for correspondence:
Chong-an Di
e-mail: dicha@iccas.ac.cn
Wei Xu
e-mail: wxu@iccas.ac.cn
Daoben Zhu
e-mail: zhudb@iccas.ac.cn

Electronic supplementary material is available at http://dx.doi.org/10.1098/rsta.2013.0008 or via http://rsta.royalsocietypublishing.org.

Royal Society Publishing

Inkjet-printed flexible organic thin-film thermoelectric devices based on p- and n-type poly(metal 1,1,2,2-ethenetetrathiolate)s/polymer composites through ball-milling

Fei Jiao, Chong-an Di, Yimeng Sun, Peng Sheng, Wei Xu and Daoben Zhu

Beijing National Laboratory for Molecular Sciences, Laboratory of Organic Solids, Institute of Chemistry, Chinese Academy of Sciences, Beijing 100190, People's Republic of China

In this article, we put forward a simple method for the synthesis of thermoelectric (TE) composite materials. Both n- and p-type composites were obtained by ball-milling the insoluble and infusible metal coordination polymers with other polymer solutions. The particle size, film morphology and composition were characterized by dynamic light scattering, scanning electron microscopy, transmission electron microscopy and energy-dispersive X-ray spectroscopy. The TE properties of the drop-cast composite film were measured at different temperatures. An inkjet-printed flexible device was fabricated and the output voltage and short-circuit current at various hot-side temperatures (T_{hot}) and temperature gradients (ΔT) were tested. The composite material not only highly maintained the TE properties of the pristine material but also greatly improved its processability. This method can be extended to other insoluble and infusible TE materials for solution-processed flexible TE devices.

1. Introduction

Interest in thermoelectric (TE) materials has increased significantly in recent years. Because of their potential applications in cooling and power generation without moving parts or hazardous working fluids, TE materials have fundamental importance in terms of energy and environmental issues [1,2]. The performance of TE devices is determined by a dimensionless quantity $ZT = S^2\sigma T/\kappa$, where S, σ, κ and T are the Seebeck coefficient, electrical conductivity, thermal conductivity and the absolute temperature, respectively [3].

Persistent efforts have been made to improve ZT values since the 1950s, by using state-of-the-art high-performance TE materials that are mainly inorganic semiconductors, such as Bi_2Te_3, PbTe, clathrates, half-Heusler alloys, pentatellurides and skutterudites [3–9]. However, some issues, such as toxicity, shortage of natural resources, high cost and poor processability, with these inorganic materials are hindering their extensive applications. On the contrary, organic materials, especially conjugated polymers [10–13], are receiving more and more attention owing to their advantages of abundant resources, low-cost synthesis, mechanical flexibility and solution processability over large areas. Recently, organic conducting materials have attracted increasing interest to explore their TE properties [14–17].

In parallel to optimizing conventional TE materials and finding new ones, it is also timely and necessary to focus on device design and to seek economical manufacturing methods that will enable these materials to be used in practical applications [18]. Even if their efficiency is still not very high, they could be used in some niche applications, such as chip cooling or power generation on the microscale [19]. Large-area production processes, such as printing and coating, could substantially reduce costs in processing and manufacturing, thus creating widespread interest in the development of solution-processable TE materials [12,20,21]. In a previous study, our group found that 1,1,2,2-ethenetetrathiolate(ett)–metal coordination polymers poly[A_x(M-ett)] (A = Na, K; M = Ni, Cu) possess excellent TE properties. The ZT values of n-type poly[K_x(Ni-ett)] can reach 0.2 and p-type poly[Cu_x(Cu-ett)] 0.01 around 400 K [22]. The shortcoming of these kinds of polymers is that they are insoluble and infusible, which significantly affects their processability. A lot of work has been done to solve this problem, e.g. synthesizing composites is a good approach and can combine the advantages of each component [20,23–27]. In this work, the poly[A_x(M-ett)] composite with the best performance was obtained via ball-milling [28–33] with poly(vinylidene fluoride) (PVDF) solution. PVDF was selected as the matrix owing to its good thermal and chemical stability, non-toxicity, mechanical strength and low water absorption characteristics, which are suitable for the fabrication of electronic components [34]. Composites with other polymers, such as polymethyl acrylate (PMMA), polyacrylonitrile (PAN) and polyvinyl alcohol (PVA), were also investigated. The Seebeck coefficients and conductivities of the composite films were measured, and the performances of the inkjet-printed prototype devices [12] were also gauged.

2. Experimental details

(a) Materials

1,3,4,6-tetrathiapentalene-2,5-dione (TPD; Tci, 98%), sodium methoxide (Alfa Aesar, 98%), potassium methoxide (Alfa Aesar, 90%), nickel (II) chloride, anhydrous (Alfa Aesar, 98%) and cuprous iodide (Acros, 98%) were employed for the synthesis of metal coordination polymers. PMMA (Alfa Aesar), PVA (Aladdin reagent, degree of hydrolysis = 99.8–100%), PVDF (Sigma-Aldrich, Mw ~ 540 000), PAN (Sigma-Aldrich, Mw ~ 150 000) and polyvinyl butyral (PVB; Sigma-Aldrich) were used as the film-forming materials. *N*-methyl-2-pyrrolidone (NMP) was purchased from J&K Chemical and other reagents from Beijing Chemical Works. All reagents except methanol were of analytical grade and were directly used without further purification; methanol was of guaranteed grade.

(b) Synthesis of poly[A_x(M-ett)]

The metal coordination polymers poly[K_x(Ni-ett)] were synthesized according to previous reports [22]. In brief, TPD (7 g, 33.6 mmol) was reacted with excess potassium methoxide (11.8 g, 151.2 mmol) in refluxing methanol solution (450 ml) for 12 h under an inert atmosphere. Then $NiCl_2$ (4.41 g, 33.6 mmol in 250 ml methanol) was added and refluxed for 12 h. After stirring under air for 12 h, the precipitate was collected by filtration and rinsed thoroughly with water, methanol and diethyl ether, sequentially. Finally, the black solid was dried under vacuum for 12 h and ground into powder. Poly[Cu_x(Cu-ett)] was synthesized using a similar procedure except that the amount of CuI was 3.5 equivalents.

(c) Composite preparation

The poly[A_x(M-ett)] composites were obtained via ball-milling with different polymer solutions. Poly[K_x(Ni-ett)]/PVDF composite, for example, was prepared in accordance with the following steps: first, PVDF was dissolved in dimethyl sulfoxide (DMSO) at 353 K for 4 h under continuous agitation using a magnetic stirrer in an Erlenmeyer flask to form a 20 mg ml^{-1} solution; second, the solution (10 ml) and the poly[K_x(Ni-ett)] powder (0.4 g) were placed into an agate jar (50 ml) with 70 agate balls (diameter = 5 mm); finally, the mixture was milled at a rotating velocity of 600 r.p.m. for 24 h using a planetary ball mill (XQM-0.4L, Nanjing University of Technology, People's Republic of China). Other composites with different kinds of polymer solutions and with different mass ratios were prepared using a similar procedure to the one mentioned above.

(d) Device fabrication

An all-polymer TE module consisting of six thermocouples was fabricated according to the structure illustrated in figure 1*a*. First, polyethylene terephthalate (PET) substrate was ultrasonically cleaned with deionized water, ethanol and acetone, sequentially, then dried at 353 K. Then p- and n-type composite films (with a thickness of 2–5 μm) were inkjet printed onto the PET substrate using a Jetlab II inkjet-printing system, with an 80 μm nozzle, and dried at 363 K for 10 h. Finally, a 100 nm gold electrode was vacuum deposited, finalizing the module fabrication. A photograph of the module obtained is shown in figure 1*b*.

(e) Characterization

The morphology of the composites was characterized by transmission electron microscopy (TEM) using a JEOL 1011 microscope and scanning electron microscopy (SEM) using an S-4800 microscope (Hitachi). Energy-dispersive X-ray spectroscopy (EDS) was used on an S-4800 scanning electron microscope at an accelerating voltage of 15 kV, for analysis of the film composition. The average particle size was measured by dynamic light scattering (DLS) using a Zetasizer Nano ZS (Malvern Instruments, Malvern, UK). X-ray photoelectron spectroscopy (XPS) data were obtained with an ESCALab220i-XL electron spectrometer (VG Scientific) using 300 W Al Kα radiation.

Free-standing composite films were prepared by casting the composite slurry on pretreated glass substrates, followed by drying under a vacuum at 343–383 K for 10 h. The films were cut into rectangular bars with the approximate dimensions of $3 \times 5\ mm^2$, then they were mounted on the measuring boards (four patterned Ag lines on glass) and fixed by silver conductive paint (SCP03B; Electrolube). After the silver paste had dried, the samples were placed in a TPS refrigerator and the electrical resistance in a temperature range of 260–400 K was measured by the standard four-probe method using a Keithley 2002 multimeter. The electrical conductivity was calculated using $\sigma = l/RWT$, where l is the length of film between the inner two electrodes, R is the resistance, and W and T are the film width and thickness, respectively.

Seebeck coefficients were measured using the integral method and constantan wire was used as a reference material. Before testing, the sample film and the constantan wire were

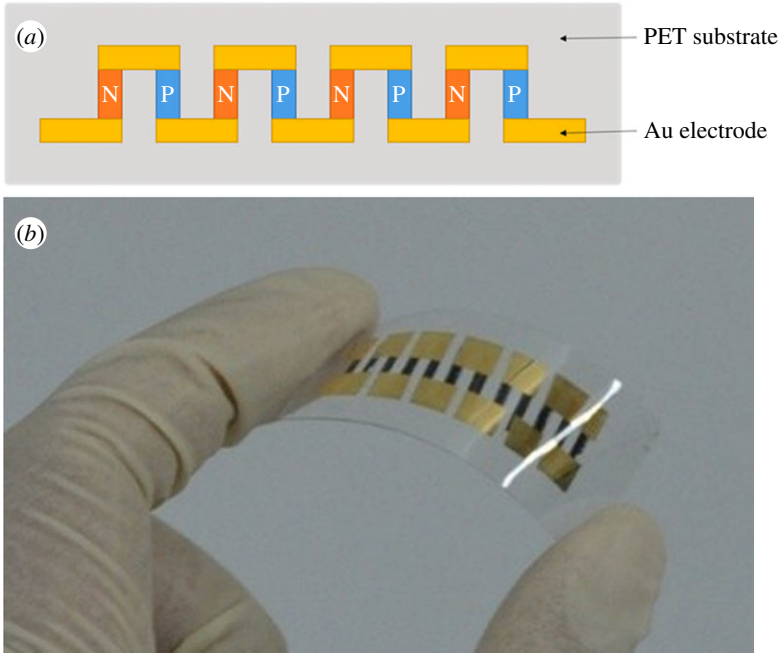

Figure 1. (*a*) Schematic and (*b*) image of a six-leg inkjet-printed composite TE device on a flexible PET substrate.

symmetrically adhered to the measuring boards using silver conductive paint (SCP03B; Electrolube). After the silver paste had dried, samples were placed in a temperature-variable Dewar (MMR Tech.) and evacuated. Under vacuum below 10 mtorr, Seebeck coefficients were measured by means of a SB-100 Seebeck measurement system (MMR Tech.) in a temperature range of 260–400 K.

Dark current versus voltage (I–V), which was used to calculate output voltage and short-circuit current of the prototype devices, was obtained under a vacuum using a semiconductor characterization system (Keithley 4200-SCS). The applied voltage was varied from −0.1 to 0.1 V in steps of 0.5 mV. Temperature gradients were created by a hot and a cold plate and were measured by platinum resistance thermometers.

3. Results and discussion

Figure 2 shows SEM images of the composite film. Combined with EDS (see electronic supplementary material, figure S2), it can be seen that, for both Ni and Cu composites, no obvious boundary is visible between the coordination polymers and PVDF. The difference is that there are some aggregated large particles on the surface of the poly[Cu_x(Cu-ett)]/PVDF film resulting in a greater decrease in conductivity in Cu composites. The average particle size for n- and p-type composites is approximately 456–850 nm and 229–414 nm, respectively, which can be seen in the electronic supplementary material, figure S1. The particle size and morphology were also confirmed by the TEM images, as depicted in figure 3. In these TEM images, it can be seen that the particles interconnected with each other to form long chains with a length greater than 10 μm, which provides the charge transport pathway in the composites. To further explore the coordination environment changes of the central metals before and after ball-milling, we performed XPS experiments (see the electronic supplementary material, figure S3). For poly[K_x(Ni-ett)] and its composite, peaks of Ni2p3/2 appeared at both 853.7 and 855.8 eV, and the ratio of the two peaks was the same (1.97). These results reveal that there is no oxidation during the ball-milling process for the n-type composites. For poly[Cu_x(Cu-ett)], the binding energy of Cu2p3/2 peaks at 932.9 and 934.4 eV, but for its composite the two peaks lie at 932.5

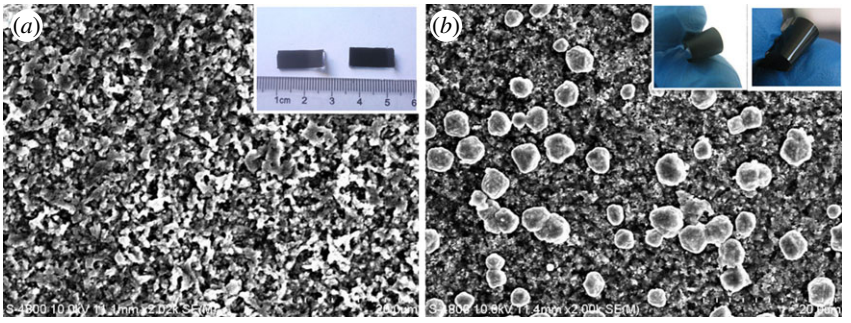

Figure 2. SEM images of (*a*) n-type and (*b*) p-type composite films. Insets in (*a*) and (*b*) are photographs of composite films on a glass substrate and self-standing; the left is n-type and the right is p-type material.

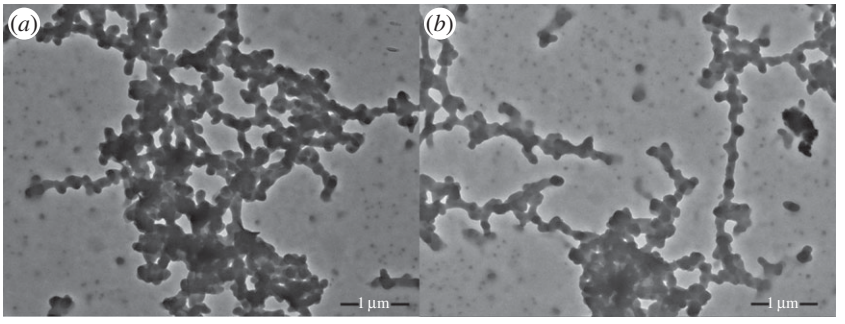

Figure 3. TEM images of (*a*) n-type and (*b*) p-type composites.

and 934.4 eV. And the ratio of the two peaks is different, 4.7 and 13.6, respectively. The change in the binding environment of Cu atoms should be another factor leading to the conductivity decrease in Cu composites.

It was found that the drying temperature also affected the TE properties of n- and p-type composite films. As shown in figure 4, for poly[K_x(Ni-ett)]/PVDF composite films, both the electrical conductivity and Seebeck coefficient increase, and then decline, as the drying temperature increases, with a maximum value of approximately 2.0 S cm^{-1} and $-36\,\mu$V K^{-1} obtained with the sample dried at 363 K. As the thermal conductivity of PVDF [35] is lower than that of poly[K_x(Ni-ett)] and poly[Cu_x(cu-ett)], it is expected that the composites should possess lower thermal conductivities than the pristine coordination polymers. Here, the thermal conductivity of the composite films was not determined. So, we estimated performances of the composite films with the TE power factor ($PF = \sigma S^2$) instead of the ZT value. Optimized PF can reach 0.26 μW m^{-1} K^{-2} at 400 K with the samples dried at 363 K. For poly[Cu_x(Cu-ett)]/PVDF composites, the conductivity increases whereas the Seebeck coefficient decreases with higher drying temperature, with a maximum PF of 0.33 μW m^{-1} K^{-2} at 400 K obtained with samples dried at 363 K.

The TE properties of the composite films with different amounts of coordination polymer to PVDF weight ratios were also investigated, as shown in figure 5. The conductivity of both n- and p-type composite films increases when the content of the coordination polymers is increased. This can be explained by the fact that the number of conductive pathways augments with more coordination polymer loading. The Seebeck coefficient of poly[K_x(Ni-ett)]/PVDF composites increases with higher coordination polymer content whereas for poly[Cu_x(Cu-ett)]/PVDF composites it decreases; this may be owing to the fact that PVDF has a positive Seebeck coefficient that is larger than that of poly[Cu_x(Cu-ett)]. The PF can reach 1.92 and 1.58 μW m^{-1} K^{-2} at 400 K for n- and p-type composites separately at a coordination polymer to PVDF mass ratio of 2 : 1.

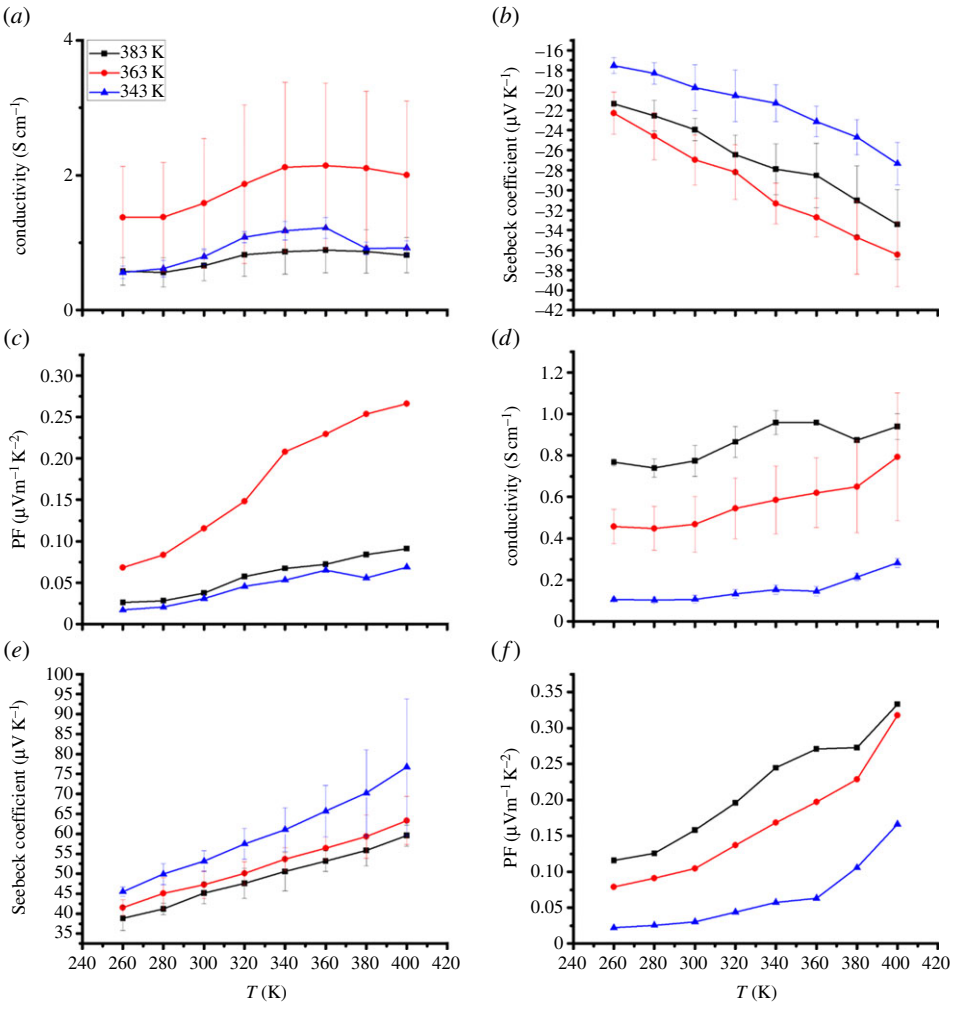

Figure 4. Temperature dependence of electrical conductivity, Seebeck coefficient and power factor for n-type poly[K_x(Ni-ett)]/PVDF/DMSO composite films (*a–c*) and p-type poly[Cu_x(Cu-ett)]/PVDF/DMSO composite films (*d–f*) prepared with different drying temperatures.

For comparison, the TE properties of the optimized composites and the pristine materials at 300 K are summarized in table 1. For both n- and p-type composite materials, the changes in the Seebeck coefficient compared with pristine materials is not so obvious. The main problem that affects the PF is the reduction in electrical conductivity, as the insulating PVDF significantly blocks the pathway for transporting carriers. Owing to the partial aggregation of poly[Cu_x(Cu-ett)] particles in the p-type composite, which can be seen in figure 2*b* (there are a lot of large particles formed on the surface of the cast thin film), the p-type composites display a greater reduction in conductivities than the n-type composite materials. Furthermore, the low density of the drop-cast films (2.2 g cm^{-3} for poly[K_x(Ni-ett)]/PVDF 1 : 1 composite and 2.39 g cm^{-3} for poly[Cu_x(Cu-ett)]/PVDF 1 : 1 composite) may also affect the TE properties of the composites [14,36]. But the exact relationship between the film density and the TE properties needs to be further explored. Although the PF of the composites is still quite low, it could be further optimized by using a conducting polymer matrix or changing the coordination polymers to inorganic TE materials with higher ZT values.

Based on these composite materials, a prototype device consisting of six thermocouples was prepared by inkjet printing, as shown in figure 1. Figure 6 shows the measured voltage and

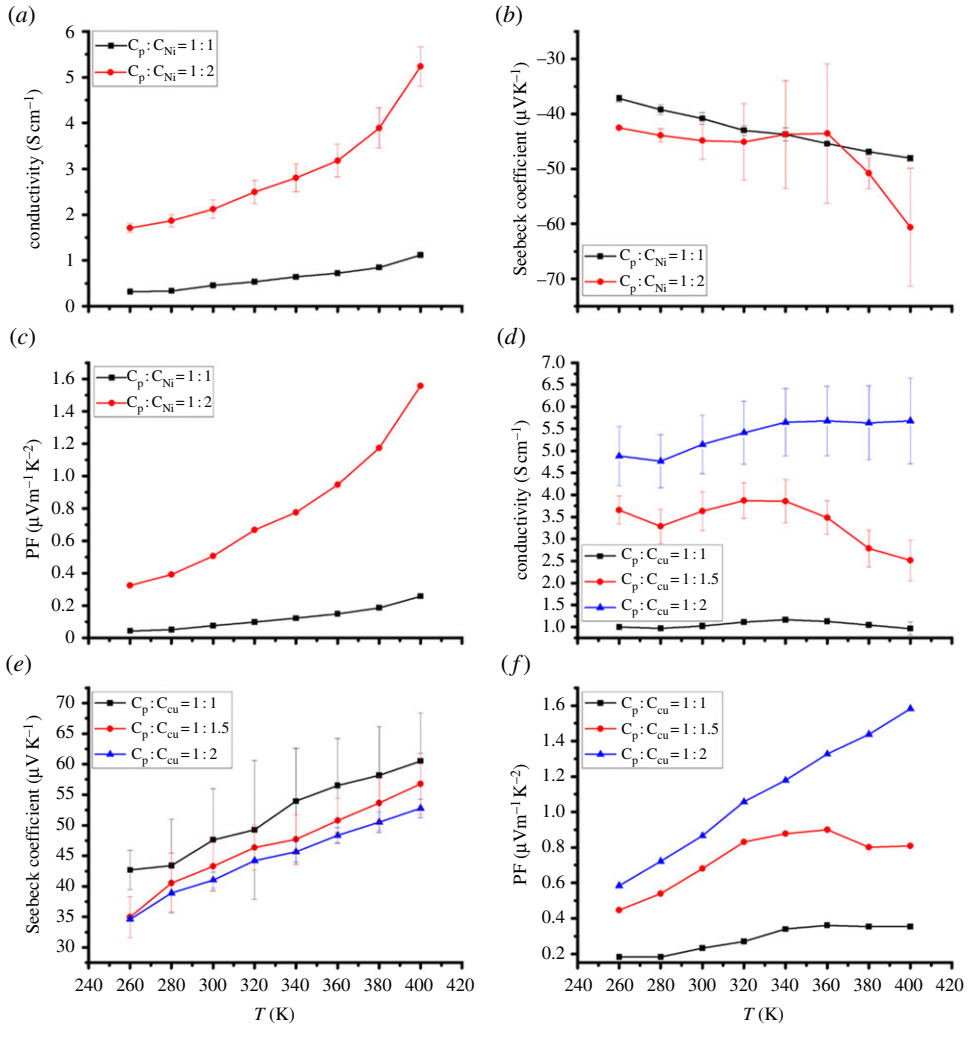

Figure 5. Temperature dependence of electrical conductivity, Seebeck coefficient and power factor for n-type poly[K_x(Ni-ett)]/PVDF/NMP composite films (*a–c*) and p-type poly[Cu_x(Cu-ett)]/PVDF/DMSO composite films (*d–f*) with different pristine material to PVDF weight ratios. In these figures, $C_p : C_{Ni}$ and $C_p : C_{Cu}$ represent the weight ratios of PVDF to poly[K_x(Ni-ett)] and poly[Cu_x(Cu-ett)] respectively.

Table 1. The electrical conductivity, Seebeck coefficient and power factor of n- and p-type composites and pristine materials at 300 K.

sample	σ (S cm^{-1})	S (μV K^{-1})	PF (μ Wm^{-1} K^{-2})
poly[K_x(Ni-ett)]/PVDF	2.12	−44.9	0.43
poly[K_x(Ni-ett)]	8.31	−67.4	3.71
poly[Cu_x(Cu-ett)]/PVDF	5.14	41.0	0.86
poly[Cu_x(Cu-ett)]	42.45	57.1	13.86

current of the device as a function of hot-side temperature. The maximum output voltage and short-circuit current of approximately 15 mV and 3 μA were obtained at 50°C ($\Delta T = 25$°C). The overall Seebeck coefficient of 95 μV K^{-1} could be calculated by a linear fit to the temperature difference/dependent voltage. The major drawback of this prototype device is that the contact

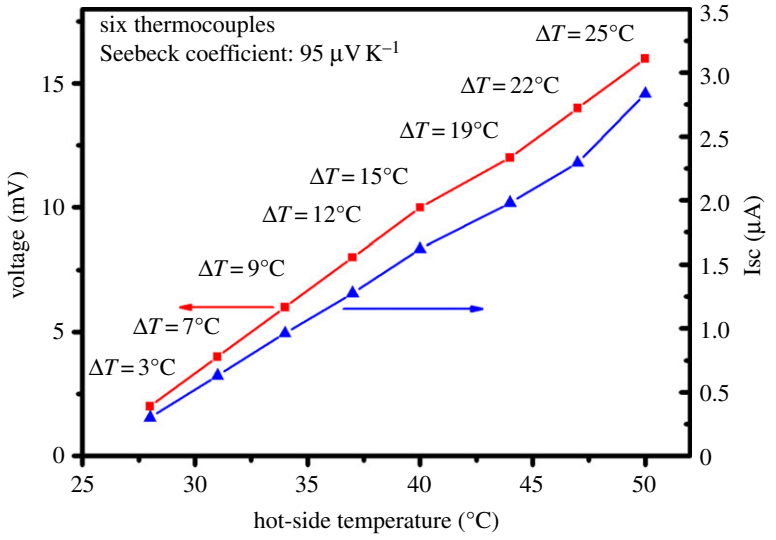

Figure 6. The output voltage and short-circuit current of the flexible device.

resistance between the TE material and device electrodes (51 Ω) is quite large compared with the resistance of the thermocouple (3.1 Ω), thus hindering the power output. The maximum output power was 45 nW with a load resistance of 5000 Ω. For higher power output, it is feasible to make flexible TE devices consisting of hundreds of p–n couples and the contact resistance remains to be further optimized.

4. Conclusion

In summary, we demonstrate a facile, efficient and general strategy to prepare solution-processed TE composites. Specifically, both n- and p-type insoluble coordination polymers were ball-milled with other polymer solutions to form composites. A flexible TE module consisting of six thermocouples was fabricated via inkjet printing and tested. Upon the application of a 25°C temperature gradient, the TE voltage could reach 15 mV. Although the efficiency is still much lower than state-of-the-art inorganic materials, it could be further increased by device optimization and using an intrinsically conductive polymer matrix. In combination with the facile synthesis and light-weight, low-cost and non-toxic properties of the composites, this manufacturing technique presents an exciting new platform for future solution-processed flexible TE generators.

Funding statement. Financial support from the Ministry of Science and Technology of China (project no.: 2013CB632506) and the Chinese Academy of Sciences is gratefully acknowledged.

References

1. Chen J *et al.* 2012 Superlow thermal conductivity 3D carbon nanotube network for thermoelectric applications. *ACS Appl. Mater. Interfaces* **4**, 81–86. (doi:10.1021/am201330f)
2. Yu C, Kim YS, Kim D, Grunlan JC. 2008 Thermoelectric behavior of segregated-network polymer nanocomposites. *Nano Lett.* **8**, 4428–4432. (doi:10.1021/nl802345s)
3. Venkatasubramanian R, Siivola E, Colpitts T, O'Quinn B. 2001 Thin-film thermoelectric devices with high room-temperature figures of merit. *Nature* **413**, 597–602. (doi:10.1038/35098012)
4. Harman TC, Taylor PJ, Walsh MP, LaForge BE. 2002 Quantum dot superlattice thermoelectric materials and devices. *Science* **297**, 2229–2232. (doi:10.1126/science.1072886)

5. Hsu KF *et al.* 2004 Cubic $AgPb_mSbTe_{2+m}$: bulk thermoelectric materials with high figure of merit. *Science* **303**, 818–821. (doi:10.1126/science.1092963)
6. Littleton RT, Tritt TM, Kolis JW, Ketchum DR. 1999 Transition-metal pentatellurides as potential low-temperature thermoelectric refrigeration materials. *Phys. Rev. B* **60**, 13 453–13 457. (doi:10.1103/PhysRevB.60.13453)
7. Mastronardi K, Young D, Wang CC, Khalifah P, Cava RJ, Ramirez AP. 1999 Antimonides with the half-Heusler structure: new thermoelectric materials. *Appl. Phys. Lett.* **74**, 1415–1417. (doi:10.1063/1.123596)
8. Yan X *et al.* 2010 Experimental studies on anisotropic thermoelectric properties and structures of n-type $Bi_2Te_{2.7}Se_{0.3}$. *Nano Lett.* **10**, 3373–3378. (doi:10.1021/nl101156v)
9. Nolas GS, Cohn JL, Slack GA, Schujman SB. 1998 Semiconducting Ge clathrates: promising candidates for thermoelectric applications. *Appl. Phys. Lett.* **73**, 178–180. (doi:10.1063/1.121747)
10. Toshima N. 2002 Conductive polymers as a new type of thermoelectric material. *Macromol. Symp.* **186**, 81–86. (doi:10.1002/1521-3900(200208)186:1<81::AID-MASY81>3.0.CO;2-S)
11. Taggart DK, Yang Y, Kung S-C, McIntire TM, Penner RM. 2011 Enhanced thermoelectric metrics in ultra-long electrodeposited PEDOT nanowires. *Nano Lett.* **11**, 125–131. (doi:10.1021/nl103003d)
12. Bubnova O, Khan ZU, Malti A, Braun S, Fahlman M, Berggren M, Crispin X. 2011 Optimization of the thermoelectric figure of merit in the conducting polymer poly(3,4-ethylenedioxythiophene). *Nat. Mater.* **10**, 429–433. (doi:10.1038/nmat3012)
13. Zhang Q, Sun YM, Xu W, Zhu DB. 2012 Thermoelectric energy from flexible P3HT films doped with a ferric salt of triflimide anions. *Energy Environ. Sci.* **5**, 9639–9644. (doi:10.1039/c2ee23006b)
14. Bubnova O, Crispin X. 2012 Towards polymer-based organic thermoelectric generators. *Energy Environ. Sci.* **5**, 9345–9362. (doi:10.1039/c2ee22777k)
15. Bubnova O, Berggren M, Crispin X. 2012 Tuning the thermoelectric properties of conducting polymers in an electrochemical transistor. *J. Am. Chem. Soc.* **134**, 16 456–16 459. (doi:10.1021/ja305188r)
16. Poehler TO, Katz HE. 2012 Prospects for polymer-based thermoelectrics: state of the art and theoretical analysis. *Energy Environ. Sci.* **5**, 8110–8115. (doi:10.1039/c2ee22124a)
17. Dubey N, Leclerc M. 2011 Conducting polymers: efficient thermoelectric materials. *J. Polym. Sci. Part B: Polym. Phys.* **49**, 467–475. (doi:10.1002/polb.22206)
18. Zebarjadi M, Esfarjani K, Dresselhaus MS, Ren ZF, Chen G. 2012 Perspectives on thermoelectrics: from fundamentals to device applications. *Energy Environ. Sci.* **5**, 5147–5162. (doi:10.1039/c1ee02497c)
19. Zhang B, Sun J, Katz HE, Fang F, Opila RL. 2010 Promising thermoelectric properties of commercial PEDOT:PSS materials and their Bi_2Te_3 powder composites. *ACS Appl. Mater. Interfaces* **2**, 3170–3178. (doi:10.1021/am100654p)
20. See KC, Feser JP, Chen CE, Majumdar A, Urban JJ, Segalman RA. 2010 Water-processable polymer-nanocrystal hybrids for thermoelectrics. *Nano Lett.* **10**, 4664–4667. (doi:10.1021/nl102880k)
21. Wüsten J, Potje-Kamloth K. 2008 Organic thermogenerators for energy autarkic systems on flexible substrates. *J. Phys. D: Appl. Phys.* **41**, 135113. (doi:10.1088/0022-3727/41/13/135113)
22. Sun Y, Sheng P, Di C, Jiao F, Xu W, Qiu D, Zhu D. 2012 Organic thermoelectric materials and devices based on p- and n-type poly(metal 1,1,2,2-ethenetetrathiolate)s. *Adv. Mater.* **24**, 932–937. (doi:10.1002/adma.201104305)
23. Yamamoto T, Kubota E, Taniguchi A, Dev S, Tanaka K, Osakada K, Sumita M. 1992 Electrically conductive metal sulfide polymer composites prepared by using organosols of metal sulfides. *Chem. Mater.* **4**, 570–576. (doi:10.1021/cm00021a015)
24. Meng C, Liu C, Fan S. 2010 A promising approach to enhanced thermoelectric properties using carbon nanotube networks. *Adv. Mater.* **22**, 535–539. (doi:10.1002/adma.200902221)
25. Yu C, Choi K, Yin L, Grunlan JC. 2011 Light-weight flexible carbon nanotube based organic composites with large thermoelectric power factors. *ACS Nano* **5**, 7885–7892. (doi:10.1021/nn202868a)
26. Yao Q, Chen L, Zhang W, Liufu S, Chen X. 2010 Enhanced thermoelectric performance of single-walled carbon nanotubes/polyaniline hybrid nanocomposites. *ACS Nano* **4**, 2445–2451. (doi:10.1021/nn1002562)

27. Kim YS, Kim D, Martin KJ, Yu C, Grunlan JC. 2010 Influence of stabilizer concentration on transport behavior and thermopower of CNT-filled latex-based composites. *Macromol. Mater. Eng.* **295**, 431–436.
28. Ge Z-H, Zhang B-P, Shang P-P, Yu Y-Q, Chen C, Li J-F. 2011 Enhancing thermoelectric properties of polycrystalline Bi_2S_3 by optimizing a ball-milling process. *J. Electron Mater.* **40**, 1087–1094. (doi:10.1007/s11664-011-1548-6)
29. Zhang SN, He J, Ji XH, Su Z, Yang SH, Zhu TJ, Zhao XB, Tritt TM. 2009 Effects of ball-milling atmosphere on the thermoelectric properties of TAGS-85 compounds. *J. Electron Mater.* **38**, 1142–1147. (doi:10.1007/s11664-009-0779-2)
30. Schilz J, Riffel M, Pixius K, Meyer HJ. 1999 Synthesis of thermoelectric materials by mechanical alloying in planetary ball mills. *Powder Technol.* **105**, 149–154. (doi:10.1016/S0032-5910(99)00130-8)
31. Lin S-S, Liao C-N. 2011 Effect of ball milling and post treatment on crystal defects and transport properties of $Bi_2(Se,Te)_3$ compounds. *J. Appl. Phys.* **110**, 093707-1–093707-7.
32. Anno H *et al.* 2009 Preparation of conducting polyaniline-bismuth nanoparticle composites by planetary ball milling. *J. Electron Mater.* **38**, 1443–1449. (doi:10.1007/s11664-009-0786-3)
33. Bottger PHM, Valset K, Deledda S, Finstad TG. 2010 Influence of ball-milling, nanostructuring, and Ag inclusions on thermoelectric properties of ZnSb. *J. Electron. Mater.* **39**, 1583–1588. (doi:10.1007/s11664-010-1269-2)
34. Zhou W, Zuo J, Ren W. 2012 Thermal conductivity and dielectric properties of Al/PVDF composites. *Compos. Part A: Appl. Sci. Manufac.* **43**, 658–664. (doi:10.1016/j.compositesa.2011.11.024)
35. Iguchi CY, dos Santos WN, Gregorio Jr R. 2007 Determination of thermal properties of pyroelectric polymers, copolymers and blends by the laser flash technique. *Polym. Test.* **26**, 788–792. (doi:10.1016/j.polymertesting.2007.04.009)
36. Yan H, Sada N, Toshima N. 2002 Thermal transporting properties of electrically conductive polyaniline films as organic thermoelectric materials. *J. Therm. Anal. Calorimetry* **69**, 881–887. (doi:10.1023/A:1020612123826)